nature physics

LETTERS

PUBLISHED ONLINE: 25 JULY 2016 | DOI: 10.1038/NPHYS3833

Fermi-level-dependent charge-to-spin current conversion by Dirac surface states of topological insulators

K. Kondou[1]*, R. Yoshimi[2], A. Tsukazaki[3], Y. Fukuma[1,4], J. Matsuno[1], K. S. Takahashi[1], M. Kawasaki[1,2], Y. Tokura[1,2] and Y. Otani[1,5]

Spin–momentum locking in the Dirac surface state of a topological insulator (TI)[1–6] offers a distinct possibility for highly efficient charge-to-spin current (C–S) conversion compared with spin Hall effects in conventional paramagnetic metals[7–13]. For the development of TI-based spin current devices, it is essential to evaluate this conversion efficiency quantitatively as a function of the Fermi level position E_F. Here we introduce a coefficient q_{ICS} to characterize the interface C–S conversion effect by means of the spin torque ferromagnetic resonance (ST-FMR) for $(Bi_{1-x}Sb_x)_2Te_3$ thin films as E_F is tuned across the bandgap. In bulk insulating conditions, the interface C–S conversion effect via the Dirac surface state is evaluated as having large, nearly constant values of q_{ICS}, reflecting that q_{ICS} is inversely proportional to the Fermi velocity v_F, which is almost constant. However, when E_F traverses through the Dirac point, the q_{ICS} is remarkably reduced, possibly due to inhomogeneity of k_F and/or instability of the helical spin structure. These results demonstrate that fine tuning of E_F in TI-based heterostructures is critical in maximizing the efficiency using the spin–momentum locking mechanism.

Three-dimensional topological insulators (TIs) possess metallic surface states in which the spins of carriers are locked orthogonal to their momenta as a result of the time-reversal invariant. This feature is called 'spin–momentum locking', and has been employed as the principal mechanism to induce spin accumulation in the surface states of TIs (refs 1,3–5,14–17). Conceptually, the charge current can fully contribute to the spin current via spin–momentum locking; a C–S conversion efficiency θ_{CS} of 100% is expected at the non-TI/TI heterointerface. This highly efficient C–S conversion can be widely applicable to spintronic devices. However, the C–S conversion efficiency deduced from the spin torque measurement can exceed 100% for TIs with E_F located in the bulk band, leading to mixed contributions from the surface and bulk bands[3,4], when the efficiency is defined as $\theta_{CS} = J_S/J_C$, where J_S is the spin current density (A m^{-2}) and J_C is the charge current density (A m^{-2}) in the entire TI layer. Here we isolate the contribution of the Dirac electrons in the C–S conversion process and clarify the role of the Fermi level E_F and the Fermi velocity v_F by employing TI samples with various E_F positions. Accordingly, we define the interface C–S conversion coefficient q_{ICS} as $q_{ICS} = J_S/j_C$, where j_C is the surface charge current density (A m^{-1}). Based on the concept of spin–momentum locking, the magnitude of J_S is governed by that of j_C, which is linked with the conductivity of the surface states on the TI layer depending on the Fermi energy and Dirac dispersion: the Fermi velocity v_F and the Fermi wavevector k_F (refs 15–17). In this study, we quantitatively evaluate the interface C–S conversion effect by means of the ST-FMR technique for 8-nm $(Bi_{1-x}Sb_x)_2Te_3$/8-nm Cu/10-nm $Ni_{80}Fe_{20}$ (Py) trilayer films, as shown in Fig. 1a. Systematic control of the Fermi levels by varying x in $(Bi_{1-x}Sb_x)_2Te_3$ (BST) thin films enables us to investigate the relationship between q_{ICS} and the transport properties at the surface state.

The ST-FMR technique has been routinely employed to evaluate the spin current induced via the spin Hall effect in paramagnetic metals[10]. Here we apply this technique to characterize quantitatively the interface C–S conversion effect due to spin–momentum locking in Cu-inserted TI-based trilayer heterostructures, as shown in the top schematic of Fig. 1a. On insertion of a Cu layer between the TI and ferromagnet layers, spin accumulation at the surface states can be separately evaluated owing to suppression of the exchange coupling between the ferromagnet and the surface states of TI (refs 18–20). In addition, the deposition of Cu on BST probably plays a minor role in varying the surface state condition, such as through an energy shift of the Dirac point and valence band maximum[21], owing to a similar magnitude between work function of Cu and the electron negativity of BST. A photo of the device and measurement circuit is shown at the bottom of Fig. 1a. To evaluate $q_{ICS} = J_S/j_C$ by means of ST-FMR, the charge current distribution in the trilayer should be clarified numerically, because j_C in the TI layer is one of the dominant factors in this evaluation technique. When a radiofrequency (rf) current flows in the trilayer film, FMR is excited in the top Py layer under an external static magnetic field H_{ext}. Owing to the presence of the highly conductive Cu layer, the peak of the current density is located towards the outside of the Py layer so that homogeneous rf fields (H_{rf}) can be applied to the Py layer (see Supplementary Information 1), providing better conditions for characterizing the C–S conversion effect by means of ST-FMR[22]. Accumulation of spins takes place simultaneously in the surface state of the TI; these accumulated spins generate a spin current J_S in the orthogonal direction, diffusing into both Cu and Py layers, and thus exert a spin torque on the Py layer (white arrow in Fig. 1a). Note that the spin pumping effect, as an inverse effect to the charge-to-spin conversion, provides a small contribution in the evaluation of q_{ICS} (Supplementary Information 8). A typical ST-FMR spectrum is shown in Fig. 1b: the symmetric voltage

[1]RIKEN Center for Emergent Matter Science (CEMS), Wako 351-0198, Japan. [2]Department of Applied Physics and Quantum-Phase Electronics Center (QPEC), University of Tokyo, Tokyo 113-8656, Japan. [3]Institute for Materials Research, Tohoku University, Sendai 980-8577, Japan. [4]Frontier Research Academy for Young Researchers, Kyushu Institute of Technology, Iizuka 820-8502, Japan. [5]Institute for Solid State Physics, University of Tokyo, Kashiwa 277-8581, Japan. *e-mail: kkondou@riken.jp

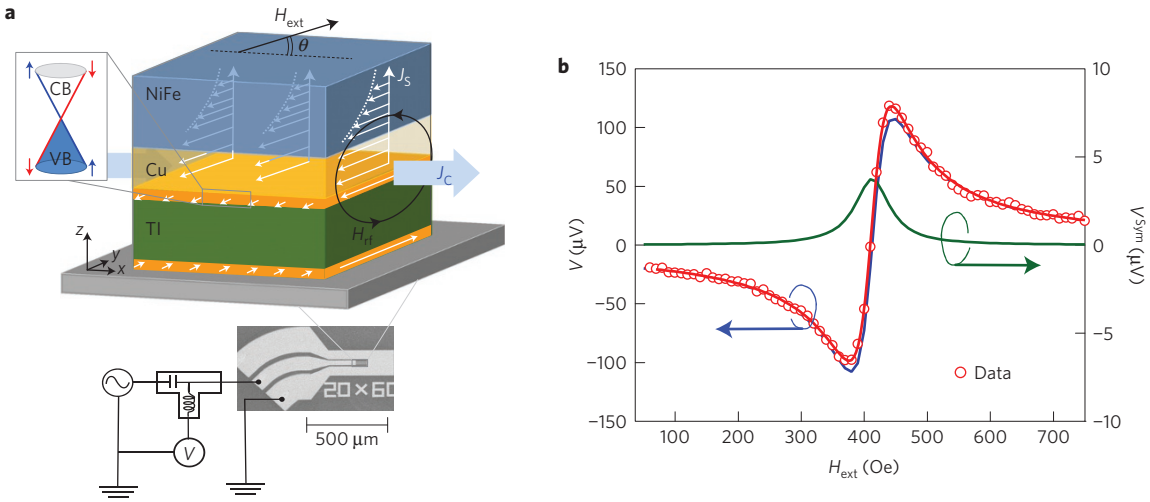

Figure 1 | Spin current generation and detection in BST/Cu/Py trilayer structure. a, ST-FMR measurement circuit and device design employing BST/Cu/Py heterostructures. White arrows on the surfaces of the BST layer show the polarization direction of spin accumulation. The static magnetic field (H_{ext}) is tilted by $\theta = 45°$. **b**, A typical ST-FMR spectrum measured for a BST ($x = 0.7$)/Cu/Py trilayer film at 10 K. Red plot shows the experimental spectrum, which can be divided into symmetric (V^{Sym}, green line) and anti-symmetric (V^{Anti}, blue line) parts. V^{Sym} and V^{Anti} correspond to spin-current-induced FMR and Oersted-field-induced FMR, respectively.

V^{Sym} is attributable to the spin torque $\tau_{\parallel}$/ corresponding to the spin current density J_S (details discussed later). By quantitative evaluation of V^{Sym}, we can deduce the interface C–S conversion coefficient q_{ICS}.

Figure 2a shows the Hall coefficients R_H obtained for seven films having different Sb composition x at 10 K. The value of R_H is negative for $x = 0$, with an increasing magnitude as x is increased to 0.82, indicating n-type conduction and a reduction in the electron density. The polarity of R_H abruptly reverses its sign when x reaches a value of approximately 0.84, revealing that the Fermi energy traverses the Dirac point (DP). In the range $0.88 \leq x \leq 1$, the polarity of R_H is positive, indicating p-type conduction. The charge carrier densities and mobilities shown in Fig. 2b are estimated from the R_H values. Compared to the previous studies[3,23], the charge carrier density in the surface state reaches as low as 10^{12} cm^{-2}, indicating that E_F is finely tuned close to the Dirac point. The mobility (μ) in BST films with $x = 0.88$ reaches a maximum value of 1,900 cm^2 V^{-1} s^{-1}, which is comparable to the previous results[24]. These transport properties and the temperature dependence of the resistivity (Supplementary Information 10) ensure that the Fermi level of BST is systematically varied from n- to p-type across the DP in a controlled manner, as shown in Fig. 2d.

Figure 2c shows the dependence of V^{Sym} on the Sb composition x obtained from an ST-FMR spectrum measured at an rf power of 8 mW. We confirmed that an rf power of 8 mW is low enough to ensure a linear response, with suppression of heating effects (Supplementary Information 5). The sign of V^{Sym} indicates the spin polarization direction of the spin current. We found a positive V^{Sym} in both n- and p-type BST films, which is an ideal feature of the C–S conversion via spin–momentum locking[1–6]. In the Dirac dispersion shown in Fig. 2e,f, spins on the Fermi circles of n- and p-type surface states of BSTs rotate clockwise and anti-clockwise, respectively[24]. When the electric field E_x is applied in the $-x$-direction, the Fermi circle with the chiral spin structure is shifted from the dashed circles to the solid circles by an amount proportional to E_x along k_x, as shown in Fig. 2e. When the Fermi level E_F is above the DP, the surface state of BST films has a higher population of down spins, generating spin polarization of the spin current along the $-y$-direction. When the Fermi level E_F is in the valence band of the Dirac dispersion, up spins with momenta along $+k_x$ are fewer in number than down spins with $-k_x$. Thus the accumulated spin is oriented along the same direction for both n- and p-type BST films. Note that these results are different from the case of a typical semiconductor such as GaAs[25], whose spin Hall effect exhibits a different sign, depending on the carrier type.

The values of q_{ICS} and the spin current conductivity σ_S of BST films are summarized as a function of x in Fig. 3. The value of q_{ICS} can be experimentally evaluated from the ratio of V^{Sym} to V^{Anti} in the ST-FMR spectrum. By using the conventional evaluation term $\theta_{CS} = J_S/J_C$, with assumption of a uniform J_C in the BST film regardless of E_F position, large values of θ_{CS} are obtained for $x = 0.5$, 0.7 and 0.9, consistent with previous studies[3] (Supplementary Information 9). Here, we propose a scheme for evaluation of q_{ICS} making use of j_c. In the ST-FMR process, the values of V^{Sym} and V^{Anti} correspond, respectively, to the spin-induced torque $\tau_{\parallel}$ and the Oersted-field-induced torque $\tau_{\perp}$ generated by charge current flow. These two torques per unit moment on the Py are respectively expressed as $\tau_{\parallel} = \hbar J_S/(2e\mu_0 M_S t_{Py})$ and $\tau_{\perp} = \xi\{J_C^{Cu} t_{Cu}/2 + j_C/2\}$, where M_S, t and ξ are the saturation magnetization, film thickness, and reduction factor of the rf field. Note that V^{Anti} shows a $\sin 2\theta \cos\theta$ dependence on the rotation angle of the applied magnetic field (Supplementary Information 6), indicating that V^{Anti} originates purely from the Oersted field. The value of ξ is calculated numerically by means of a finite element method (see Supplementary Information 1). The value of q_{ICS} can thus be given by

$$q_{ICS} \equiv \left(\frac{J_S}{j_C}\right) = \left(\frac{\tau_{\parallel}}{\tau_{\perp}}\right) \frac{a\xi t_{Py} t_{Cu} e\mu_0 M_S\{1 + M_S/H_{ext}\}^{0.5}}{\hbar t_{BST}}$$
$$= \left(\frac{V^{Sym}}{V^{Anti}}\right) \frac{a\xi t_{Py} t_{Cu} e\mu_0 M_S\{1 + M_S/H_{ext}\}^{0.5}}{\hbar t_{BST}} \quad (1)$$

where a is the ratio of J_C^{Cu} (A m^{-2}) to j_C. The spin current density into Py J_S^{Py} (A m^{-2}) is proportional to the spin accumulation at the surface state of the TI, $\langle \delta S_0 \rangle$, which is expressed as

$$\langle \delta S_0 \rangle = \frac{\hbar}{2} k_F \delta k_x = \frac{e k_F E_x \tau}{2} = \frac{\mu k_F^2 \hbar E_x}{2 v_F} \quad (2)$$

where k_F is the Fermi wavenumber, δk_x is the shift of Fermi circle, and τ is the relaxation time. In the two-dimensional system, k_F^2 is proportional to the carrier density. Therefore, $\langle \delta S_0 \rangle$ reduces to

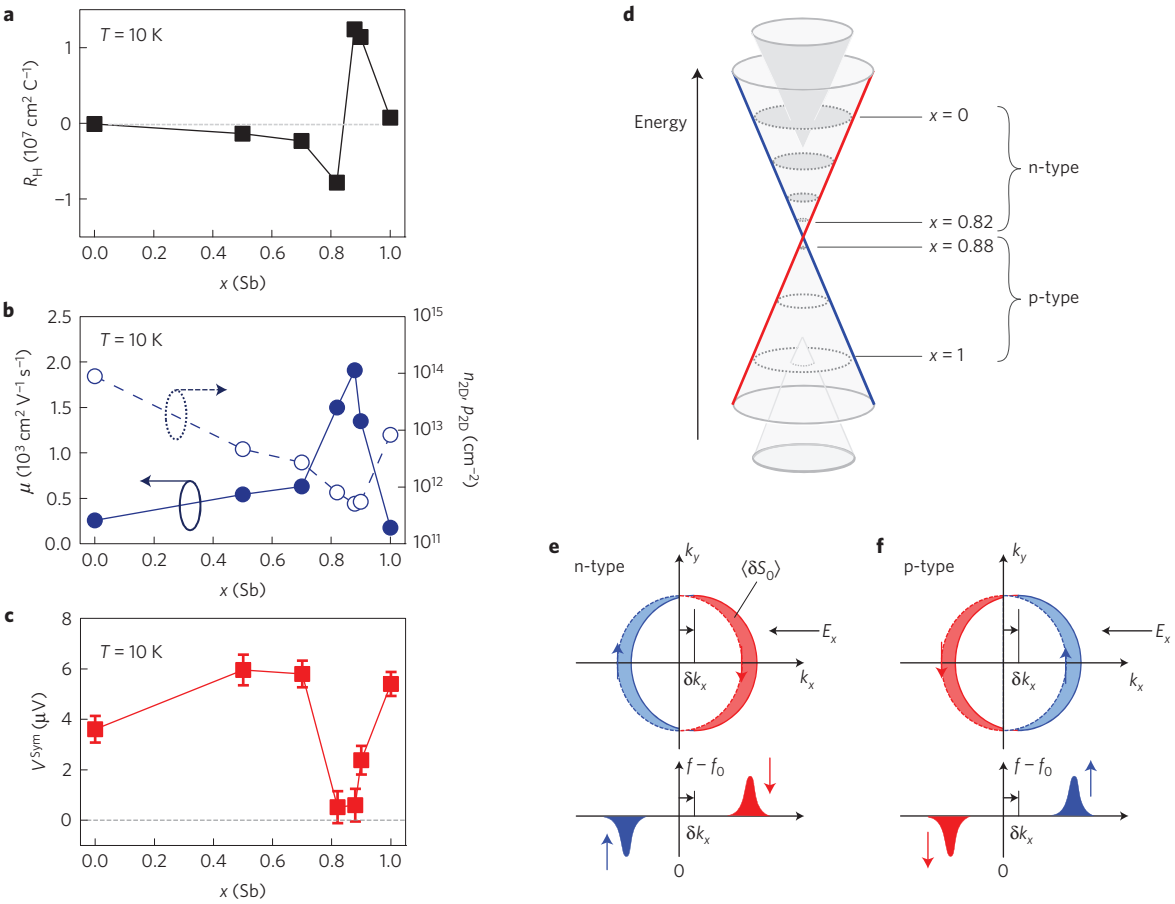

Figure 2 | Transport properties of BST films and detected V^{Sym} as a function of Sb composition. a, Hall coefficient R_H for BST films measured at 10 K. **b**, Mobility μ and carrier density n_{2D}, p_{2D} as a function of Sb composition at 10 K. **c**, Symmetric voltage of ST-FMR as a function of Sb composition. The input rf frequency and power are 7 GHz and 10 dBm, respectively. The error bars are the standard deviation from five samples with different dimensions. **d**, Schematic of the energy dispersion in BST. **e**,**f**, (Top) Spin accumulation due to a Fermi circle shift at the surface state of n-type (**e**) and p-type (**f**) BST. Solid and dashed circles are the Fermi circles with E_x and without E_x, respectively. (Bottom) Difference in the Fermi distribution ($f - f_0$) on applying an electric field.

$\hbar j_C/2ev_F$ and $q_{ICS} = J_S^{Py}/j_C \propto v_F^{-1}$ is obtained. According to angle-resolved photoemission spectra, v_F in BST increases slightly from 3.6 to 3.9 $\times$ 10^5 m s^{-1} as the Sb composition x increases from 0.5 to 0.9 (ref. 26), suggesting that q_{ICS} is almost constant in this composition range. For bulk insulating BST films with $x = 0.5$, 0.7 and 0.9 (apart from two samples in the vicinity of the DP) we observed that the values of q_{ICS} indeed lie within the range 0.45–0.57 nm^{-1}, similar in magnitude to the previous results of ST-FMR measurements in Py/Bi_2Se_3 bilayer film[3]. Of particular interest is the case $x = 0.9$; although its V^{Sym} value is nearly half those of $x = 0.5$ and 0.7, as shown in Fig. 2c, the q_{ICS} value is still comparable owing to the correction by the small j_C. Since we assume the surface thickness responsible for j_C to be 1 nm, the value of θ_{CS} is estimated to be 45 to 57% for these BST films, yielding a much higher conversion efficiency than those in typical transition metals such as β-Ta (15%) and β-W (33%) (refs 10–13). Consequently, the interface C–S conversion effect via spin–momentum locking at the surface state is evaluated fairly well using q_{ICS}, and consistent with the naive expectation of an at most 100% conversion efficiency. Note that the estimated conversion efficiency θ_{CS} is proportional to the conducting channel thickness, which contributes to J_C; therefore, the large values of θ_{CS} claimed for high conversion efficiencies in previous studies[3,4] may be overestimated by assuming a thicker conducting layer. Our estimated values of q_{ICS} less than unity appears consistent with the theoretical evaluation, which has proposed a reduction of the in-plane spin polarization due to spin–orbit entanglement in such a material with a strong spin–orbit interaction[27]. We would also like to note that the product of q_{ICS} and the inverse conversion coefficient is expected to be approximately unity for the ideal case where there is no reduction of the in-plane spin polarization in the surface state of the TI[28].

We now discuss the Fermi-level dependence of q_{ICS} shown in Fig. 3a. First, in contrast to the almost constant q_{ICS} for bulk insulating BST films with $x = 0.5$, 0.7 and 0.9, the values of q_{ICS} show a sharp dip around DP $x \sim 0.82$ and 0.88; the value of q_{ICS} decreases dramatically when E_F is located close to the DP, or equivalently k_F becomes approximately zero, originating from the almost zero V^{Sym} in our experiments (see Fig. 2c,d). Evaluated from the lowest charge carrier density of approximately 10^{12} cm^{-2}, the E_F position is located within $\pm$60 meV of the DP for $x = 0.82$ and 0.88, resulting in a small $\langle \delta S_0 \rangle$ due to the small δk_x. In such a situation, with E_F close to the DP, a finite amount of scattering may reduce the generated spin polarization, as reported in experiments with spin-resolved angular-dependent photoemission spectroscopy (ARPES)[29–31] and scanning tunnelling spectroscopy[32]. Here we give possible reasons for the reduction in the spin polarization. First, when there are inhomogeneities, such as in the Bi/Sb composition, which can be regarded as analogy to electron–hole puddles in graphene[33], in the surface state of BST around the Dirac point, charge current can flow in directions other than the electric field direction. As a result, $\langle \delta S_0 \rangle$ with various spin directions will occur in the surface state of the TI, indicating that the $\langle \delta S_0 \rangle$ in the y direction will

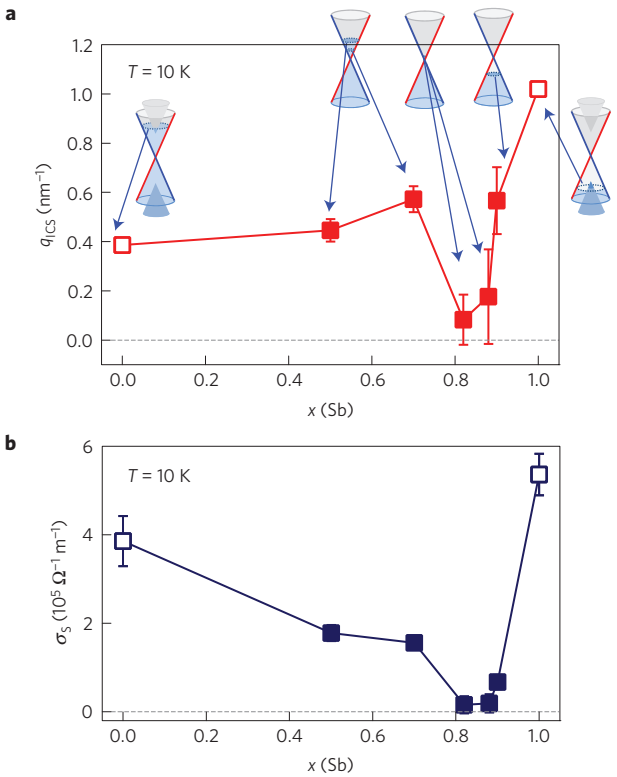

Figure 3 | Dependence of the charge-to-spin current conversion efficiency of BST on the Sb composition. a, Interface C–S conversion efficiency q_{ICS} as a function of Sb composition. Inset shows the band structure and Fermi level position for each Sb composition. Bulk insulating BST with $0.50 \leq x \leq 0.90$ should have only surface transport. Bi_2Te_3 ($x=0$) and Bi_2Sb_3 ($x=1$) have both bulk and surface conduction paths. Error bars represent the standard deviation over five samples with different dimensions. **b**, Spin current conductivity as a function of Sb composition.

decrease. Furthermore, if there is an additional surface state due to Cu deposition on the TIs, the generated spin polarization will be decreased (Supplementary Information 4). In this situation, it is likely that an ideal constant value of q_{ICS} cannot be recovered due to the almost zero V^{sym} with finite j_C. Second, for bulk conductive BST films with $x=0$ (Bi_2Te_3) and $x=1$ (Sb_2Te_3), when we apply the same analytical method as used for bulk insulating films with an assumption of a 1 nm conducting surface layer, the estimated values of q_{ICS} are found to be roughly equal to, or even twice as much as, those for the bulk insulating BST films. However, a quantitative evaluation of q_{ICS} and θ_{CS} in bulk conducting samples is fairly difficult for the following reasons. The first reason is estimation of the effects of parasitic currents: here we assume that the surface is as conductive as the bulk (see Supplementary Information 1). Considering that the surface is expected to be more conductive, the present value of q_{ICS} might be overestimated. Although the assumption of a completely insulating bulk is simplistic, a small contribution from a bulk current provides a small perturbation to the present results; we have shown an insignificant effect of the current ratio between the surface and the bulk on the evaluated values of q_{ICS} (Supplementary Information 2). The second reason is the Rashba effect: if the charge current in the bulk band also contributes to J_S via a Rashba-split band, as in Bi_2Se_3 (ref. 20), the opposite spin polarization may cancel part of the surface spin accumulation (see Supplementary Information 4). The final reason is the bulk spin Hall effect: the bulk charge current can also contribute to J_S via the ordinary spin Hall effect, of which the sign is as yet unclear.

Finally we show the spin current conductivity σ_S, defined as $\sigma_S = q_{ICS}\sigma^{surf}$, where σ^{surf} is the conductivity of the surface state of the TI, as a function of the Sb composition x in Fig. 3b. The values of σ_S in bulk insulating BST ($x=0.5$ and 0.7), excluding the DP and bulk conductive BST, take values close to $1.8 \times 10^5\ \Omega^{-1}\ m^{-1}$, which are comparable to those reported for three-dimensional processes originating from the spin Hall effect in paramagnetic metals such as Pt ($3.4 \times 10^5\ \Omega^{-1}\ m^{-1}$) (ref. 10) and β-W ($1.3 \times 10^5\ \Omega^{-1}\ m^{-1}$) (ref. 11). This high value of σ_S is certainly beneficial, not only for realizing highly efficient magnetization switching, but also for realizing non-volatile spin switching for Boolean and non-Boolean logic initially based on metal spin Hall effects[34].

Methods

Methods, including statements of data availability and any associated accession codes and references, are available in the online version of this paper.

Received 11 September 2015; accepted 20 June 2016; published online 25 July 2016

References

1. Lie, C. H. *et al*. Electrical detection of charge-current-induced spin polarization due to spin–momentum locking in Bi_2Se_3. *Nature Nanotech.* **9,** 218–224 (2014).
2. Shiomi, Y. *et al*. Spin-electricity conversion induced by spin injection into topological insulators. *Phys. Rev. Lett.* **113,** 196601 (2014).
3. Mellnik, A. R. *et al*. Spin-transfer torque generated by a topological insulator. *Nature* **511,** 449–451 (2014).
4. Fan, Y. *et al*. Magnetization switching through giant spin–orbit torque in a magnetically doped topological insulator heterostructure. *Nature Mater.* **13,** 699–704 (2014).
5. Ando, Y. *et al*. Electrical detection of the spin polarization due to charge flow in the surface state of the topological insulator $Bi_{1.5}Sb_{0.5}Te_{1.7}Se_{1.3}$. *Nano Lett.* **14,** 6226–6230 (2014).
6. Deroani, D. *et al*. Observation of inverse spin Hall effect in bismuth selenide. *Phys. Rev. B* **90,** 094403 (2014).
7. Dyakonov, M. & Perel, V. Current-induced spin orientation of electrons in semiconductors. *Phys. Lett. A* **35,** 459–460 (1971).
8. Hirsh, J. E. Spin Hall effect. *Phys. Rev. Lett.* **83,** 1834–1837 (1999).
9. Takahashi, S. & Maekawa, S. Spin current, spin accumulation and spin Hall effect. *Sci. Technol. Adv. Matter.* **9,** 014105 (2008).
10. Liu, L. *et al*. Spin-torque ferromagnetic resonance induced by the spin Hall effect. *Phys. Rev. Lett.* **106,** 036601 (2011).
11. Pai, C.-F. *et al*. Spin transfer torque devices utilizing the giant spin Hall effect of tungsten. *Appl. Phys. Lett.* **101,** 122404 (2012).
12. Liu, L. Q. *et al*. Spin torque switching with the giant spin Hall effect of tantalum. *Science* **336,** 555–558 (2012).
13. Niimi, Y. *et al*. Giant spin Hall effect induced by skew scattering from bismuth impurities inside thin film CuBi alloys. *Phys. Rev. Lett.* **109,** 156602 (2012).
14. Hasan, M. Z. & Kane, C. L. Topological insulators. *Rev. Mod. Phys.* **82,** 3045–3067 (2010).
15. Edelstein, V. M. Spin polarization of conduction electrons induced by electric current in two-dimensional asymmetric electron systems. *Solid State Commun.* **73,** 233–235 (1990).
16. Shen, K. *et al*. Microscopic theory of the inverse Edelstein effect. *Phys. Rev. Lett.* **112,** 096601 (2014).
17. Fischer, M. *et al*. Spin-torque generation in topological insulator based heterostructures. *Phys. Rev. B* **93,** 125303 (2016).
18. Wei, P. *et al*. Exchange-coupling-induced symmetry breaking in topological insulators. *Phys. Rev. Lett.* **110,** 186807 (2013).
19. Chen, C. L. *et al*. Massive Dirac fermion on the surface of a magnetically doped topological insulator. *Science* **329,** 659–662 (2010).
20. Wray, L. A. *et al*. A topological insulator surface under strong Coulomb, magnetic and disorder perturbations. *Nature Phys.* **7,** 32–37 (2011).
21. Wray, L. A. *et al*. Chemically gated electronic structure of a superconducting doped topological insulator system. *J. Phys. Conf. Ser.* **449,** 012037 (2013).
22. Yamaguchi, A. *et al*. Rectification of radio frequency current in ferromagnetic nanowire. *Appl. Phys. Lett.* **90,** 182507 (2007).
23. Lee, J. S. *et al*. Mapping the chemical potential dependence of current-induced spin polarization in a topological insulator. *Phys. Rev. B* **92,** 155312 (2015).
24. Yoshimi, R. *et al*. Dirac electron states formed at the heterointerface between a topological insulator and a conventional semiconductor. *Nature Mater.* **13,** 253–257 (2014).

25. Ando, K. *et al*. Electrically tunable spin injector free from the impedance mismatch problem. *Nature Mater.* **10,** 655–659 (2011).
26. Zhang, J. *et al*. Band structure engineering in $(Bi_{1-x}Sb_x)_2Te_3$ ternary topological insulators. *Nature Commun.* **2,** 574 (2011).
27. Yazyev, O. V. *et al*. Spin polarization and transport of surface states in the topological insulators Bi_2Se_3 and Bi_2Te_3 from first principles. *Phys. Rev. Lett.* **105,** 266806 (2010).
28. Rojas-Sánchez, J.-C. *et al*. Spin to charge conversion at room temperature by spin pumping into a new type of topological insulator: α-Sn films. *Phys. Rev. Lett.* **116,** 096602 (2016).
29. Miyamoto, M. *et al*. Topological surface states with persistent high spin polarization across the Dirac point in Bi_2Te_2Se and Bi_2Se_2Te. *Phys. Rev. Lett.* **109,** 166802 (2012).
30. Souma, S. *et al*. Spin polarization of gapped Dirac surface states near the topological phase transition in $TlBi(S_{1-x}Se_x)_2$. *Phys. Rev. Lett.* **109,** 186804 (2012).
31. Xu, S.-Y. *et al*. Unconventional transformation of spin Dirac phase across a topological quantum phase transition. *Nature Commun.* **6,** 6870 (2015).
32. Sessi, P. *et al*. Visualizing spin-dependent bulk scattering and breakdown of the linear dispersion relation in Bi_2Te_3. *Phys. Rev. B* **88,** 161407 (2013).
33. Martin, J. *et al*. Observation of electron-hole puddles in graphene using a scanning single-electron transistor. *Nature Phys.* **4,** 144–148 (2008).
34. Datta, S. *et al*. Non-volatile spin switch for Boolean and non-Boolean logic. *Appl. Phys. Lett.* **101,** 252411 (2012).

Acknowledgements

We acknowledge fruitful discussions with K. Nomura. This work was supported by Grant-in-Aid for Scientific Research on the Innovative Area, 'Nano Spin Conversion Science' (Grant No. 26103002). R.Y. is supported by the Japan Society for the Promotion of Science (JSPS) through a research fellowship for young scientists. This research was supported by the Japan Society for the Promotion of Science through the Funding Program for World-Leading Innovative R & D on Science and Technology (FIRST Program) on 'Quantum Science on Strong Correlation' initiated by the Council for Science and Technology Policy.

Author contributions

Y.O. and Y.T. conceived the project. K.K. made the devices and performed the spin torque ferromagnetic resonance measurements. R.Y. grew the topological insulator thin films and performed Hall measurements. K.K. analysed the data and wrote the manuscript with contributions from all authors. A.T., Y.F., K.S.T., J.M., M.K., Y.T. and Y.O. jointly discussed the results.

Additional information

Supplementary information is available in the online version of the paper. Reprints and permissions information is available online at www.nature.com/reprints. Correspondence and requests for materials should be addressed to K.K.

Competing financial interests

The authors declare no competing financial interests.

Methods

Sample fabrication. We grew 8-nm-thick BST films on semi-insulating InP(111) substrates by molecular beam epitaxy. The detailed growth conditions are described in a previous paper[23]. The Bi/Sb ratio was tuned by adjusting the ratio of the beam equivalent pressures of Bi and Sb. Resistivity and Hall effect measurements were carried out using small chips derived from the same samples as used for the ST-FMR measurements (see Supplementary Information 2). Thin films of 8-nm Cu/10-nm $Ni_{80}Fe_{20}$ (Py)/5-nm Al_2O_3 were grown on the BST films by e-beam evaporation at a pressure of 5×10^{-5} Pa. Al_2O_3 is used as an insulating capping layer. The resistivities of Cu and Py are measured to be 10 and 60 μΩ cm at 10 K. The BST/Cu/Py trilayer films were patterned into rectangular elements (10×30, 15×45, 20×60, 30×90, $40 \times 120\,\mu m^2$) using optical lithography and an Ar-ion etching technique. A co-planar waveguide of 5-nm Ti/200-nm Au was deposited on both sides of the rectangular elements.

ST-FMR measurement set-up. An rf current with an input power of 8 mW is applied along the long edge of the rectangle by means of a microwave analog signal generator (Keysight: MXG N5183A). An external static magnetic field H_{ext} in the range from 0 to 2.0 kOe is also applied in the film plane at an angle of $\theta = 45°$ with respect to the current flow direction. We demonstrated the rf power dependence of V^{Sym}, the heating effect, the dc current dependence of the resonance field, the frequency dependence of the half-width at half-maximum of Δ for V^{Sym} and the dependence on magnetic field angle of V^{Anti}, and concluded that the detected V^{Sym} and V^{Anti} are primarily due to the charge-to-spin conversion effect (Supplementary Information). All the experiments were performed at 10 K to measure the surface-dominant properties of TI.

Data availability. The data that support the plots within this paper and other findings of this study are available from the corresponding author upon reasonable request.